Dynamic Amyloid PET: Relationships to ^{18}F-Flortaucipir Tau PET Measures

Fabio Raman[1–4], Yu-Hua Dean Fang[1], Sameera Grandhi[1,2], Charles F. Murchison[2,5], Richard E. Kennedy[2,3], John C. Morris[6], Parinaz Massoumzadeh[7], Tammie Benzinger[7], Erik D. Roberson[2–4], and Jonathan McConathy[1,2]

[1]Department of Radiology, University of Alabama at Birmingham, Birmingham, Alabama; [2]Alzheimer's Disease Center, University of Alabama at Birmingham, Birmingham, Alabama; [3]Department of Neurology, University of Alabama at Birmingham, Birmingham, Alabama; [4]Center for Neurodegeneration and Experimental Therapeutics, University of Alabama at Birmingham, Birmingham, Alabama; [5]Department of Medicine, University of Alabama at Birmingham, Birmingham, Alabama; [6]Department of Neurology, Washington University in St. Louis School of Medicine, St. Louis, Missouri; and [7]Mallinckrodt Institute of Radiology, Washington University in St. Louis School of Medicine, St. Louis, Missouri

Measuring amyloid and predicting tau status using a single amyloid PET study would be valuable for assessing brain AD pathophysiology. We hypothesized that early-frame amyloid PET (efAP) correlates with the presence of tau pathology because the initial regional brain concentrations of radioactivity are determined primarily by blood flow, which is expected to be decreased in the setting of tau pathology. **Methods:** The study included 120 participants (63 amyloid-positive and 57 amyloid-negative) with dynamic ^{18}F-florbetapir PET and static ^{18}F-flortaucipir PET scans obtained within 6 mo of each other. These subjects were predominantly cognitively intact in both the amyloid-positive (63%) and the amyloid-negative (93%) groups. Parameters for efAP quantification were optimized for stratification of tau PET positivity, assessed by either a tauopathy score or Braak regions. The ability of efAP to stratify tau positivity was measured using receiver-operating-characteristic analysis of area under the curve (AUC). Pearson r and Spearman ρ were used for parametric and nonparametric comparisons between efAP and tau PET, respectively. Standardized net benefit was used to evaluate improvement in using efAP as an additional copredictor over hippocampal volume in predicting tau PET positivity. **Results:** Measuring efAP within the hippocampus and summing the first 3 min of brain activity after injection showed the strongest discriminative ability to stratify for tau positivity (AUC, 0.67–0.89 across tau PET Braak regions) in amyloid-positive individuals. Hippocampal efAP correlated significantly with a global tau PET tauopathy score in amyloid-positive participants ($r = -0.57$, $P < 0.0001$). Compared with hippocampal volume, hippocampal efAP showed a stronger association with tau PET Braak stage ($\rho = -0.58$ vs. -0.37) and superior stratification of tau PET tauopathy score (AUC, 0.86 vs. 0.66; $P = 0.002$). **Conclusion:** Hippocampal efAP can provide additional information to conventional amyloid PET, including estimation of the likelihood of tau positivity in amyloid-positive individuals.

Key Words: ^{18}F-florbetapir PET; ^{18}F-flortaucipir PET; early-phase PET; early-frame amyloid PET

J Nucl Med 2022; 63:287–293
DOI: 10.2967/jnumed.120.254490

Alzheimer disease (AD) is the primary cause of age-related dementia, affecting approximately 50 million people worldwide. AD pathophysiologic processes begin years before clinical symptoms. Established neuroimaging biomarkers include neurodegeneration with MRI and ^{18}F-FDG PET, as well as ^{18}F-florbetapir, ^{18}F-florbetaben, and ^{18}F-flutemetamol for amyloid plaques and ^{18}F-flortaucipir for tau tangles, respectively (*1*). These biomarkers can predict pathophysiologic progression and cognitive performance (*1*,*2*).

In standard amyloid PET studies, amyloid status is measured 30–120 min after injection, depending on the tracer (*3*,*4*). Dynamic acquisition allows collection of a second potential biomarker during the initial tracer flow–delivery phase (*5–7*), but the clinical role of these early uptake measures is not well defined. Several groups have shown strong correlations between early flow measures from dynamic amyloid PET and regional cerebral perfusion measured with ^{15}O-water PET (*6*,*8*) and between early flow measures from dynamic amyloid PET and regional cerebral glucose metabolism measured with ^{18}F-FDG (*9–11*). Other studies have shown that a higher tau burden as measured with PET correlates with regional hypometabolism observed with ^{18}F-FDG PET (*12*,*13*). This body of work led us to pursue the relationship between flow measures with dynamic amyloid PET and the presence of tau pathology.

The objectives of this study were to determine the relationship between early-frame amyloid PET (efAP) and tau PET in amyloid-positive individuals and to assess the potential of dynamic amyloid PET to predict tau PET status. We chose a relatively simple method to calculate efAP in order to increase the clinical relevance and ease of implementation. We hypothesized that reduced efAP would correlate with pathologic tau measured by PET in amyloid-positive individuals evaluated with both dynamic amyloid and tau PET scans within 6 mo of each other.

MATERIALS AND METHODS

Study Population

Participants were selected from a cohort at the Charles F. and Joanne Knight Alzheimer Disease Research Center at Washington University in St. Louis. The recruitment, assessment, and exclusion criteria methods have been published previously (*14*) and are available at https://knightadrc.wustl.edu. All studies were approved by the

Received Aug. 27, 2020; revision accepted Apr. 23, 2021.
For correspondence or reprints, contact Jonathan McConathy (jmcconathy@uabmc.edu).
Published online May 28, 2021.

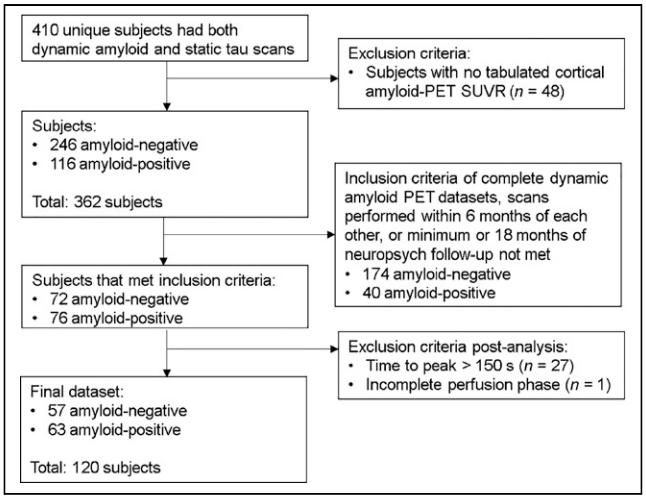

FIGURE 1. Flowchart for selection of 63 amyloid-positive and 57 amyloid-negative subjects for analysis in this study from retrospective cohort of 410 subjects.

Institutional Review Board at Washington University in St. Louis and the University of Alabama at Birmingham, indicating compliance with all ethical regulations; informed consent was obtained from all participants before study enrollment.

From the cohort of 410 unique participants, 63 amyloid-positive and 57 amyloid-negative participants who met the eligibility criteria were selected. Subjects had to have dynamic amyloid PET, tau PET, and brain MRI completed within 6 mo of each other and at least 18 mo of neuropsychologic evaluation after completion of imaging. Subjects were categorized as amyloid- and tau-positive or -negative on the basis of established cutoffs from the Charles F. and Joanne Knight Alzheimer Disease Research Center (*15*,*16*). Specifically, a mean cortical SUV ratio (SUVR) of 1.19 for amyloid PET (*16*) and a tauopathy SUVR of 1.22 for tau PET (*15*) were used to stratify amyloid and tau positivity and screen subjects on the basis of prior analyses. Subject selection and demographics, including cognitive measures, are presented in Figure 1 and Table 1, respectively.

Image Sets Used for Analysis

^{18}F-florbetapir PET was performed using an intravenous bolus of 274–418 MBq (7.4–11.3 mCi) on a Siemens Biograph mMR scanner. Data were acquired at the time of injection through 70 min, and reconstruction was performed with 26 frames (4 × 15 s, 4 × 30 s, 3 × 60 s, 3 × 120 s, 2 × 240 s, and 10 × 300 s). Data from 50 to 70 min after injection were used for amyloid quantification (*16*). Amyloid SUVRs were calculated in brain regions of interest (ROIs), using the entire cerebellum as the reference ROI.

MRI and ^{18}F-flortaucipir PET acquisition and preprocessing were performed as previously reported (*15*). Tau PET was performed on a Siemens Biograph 40 PET/CT scanner using an intravenous bolus of 266–400 MBq (7.2–10.8 mCi) of ^{18}F-flortaucipir. Data from 80 to 100 min after injection were used for regional brain tau quantification (*15*). Tau SUVRs were calculated in brain ROIs, using cerebellar gray matter as the reference ROI.

Calculation of Flow-Phase Parameters from Dynamic Amyloid PET

Regional dynamic amyloid and static tau PET data were measured using MRI-based FreeSurfer segmentation (*17*) with an algorithm (biomarker localization, analysis, visualization, extraction, and registration) developed by our group (*18*). Calculation of efAP from dynamic amyloid PET was performed in Matlab, version R2019b (MathWorks). A set of time-averaged early-frame efAP intervals was generated in Matlab to test a range of different start points (5%–50% of peak cerebral cortex radioactivity) and endpoints of early-frame intervals (45–600 s from the start of acquisition). In total, 79 target (T) ROIs based on FreeSurfer segmentation were integrated over each early-frame interval and subsequently normalized to the integrated time–activity curve of the appropriate reference (R) ROI over the same period. Since we used discrete integrals based on the radioactivity (A) and associated frame duration (D) over the selected set of early frames, the equation could be simplified as follows:

$$\mathrm{efAP_{SUVR}} = \frac{\sum_{i=\mathrm{start}}^{\mathrm{end}} (A_{Ti} D_{Ti})}{\sum_{i=\mathrm{start}}^{\mathrm{end}} (A_{Ri} D_{Ri})} \qquad \text{Eq. 1}$$

Tau Assessment in Tauopathy Summary Measure, Braak ROIs, and In Vivo Braak Staging

A tauopathy summary measure was previously experimentally derived using a sparse k-means clustering with resampling analysis to identify the ROIs most informative in dividing a cognitively normal population into high-tau and low-tau groups. The highest-weighted FreeSurfer ROIs separating these groups were the entorhinal cortex, amygdala, lateral occipital cortex, and inferior temporal cortex, and an average SUVR in these 4 ROIs was used as a summary metric for ^{18}F-flortaucipir uptake (*15*).

To replicate Braak neuropathologic staging, tau PET Braak ROIs were created from volume-weighted FreeSurfer subregions as defined by the algorithm our group developed (*18*). Braak ROIs refers to specific anatomic regions regardless of their tau status, whereas Braak staging refers to the presence of pathologic tau in these ROIs based on ^{18}F-flortaucipir PET. Similar to Schöll et al. 2016, tau PET Braak staging was performed by first categorizing the following volume-weighted, composite ROIs: transentorhinal (Braak stage I/II), limbic (Braak stage III/IV), and isocortical (Braak stage V/VI) (*19*). To maintain consistency across thresholding techniques, the same 1.22 cutoff (*15*) as was used to determine tau status was applied to the composite Braak ROIs as follows: subjects positive (SUVR > 1.22) across all 3 ROIs (Braak ROIs I/II, III/IV, and V/VI) were assigned Braak stages V and VI; subjects positive in Braak ROIs I/II and III/IV but negative in V/VI were assigned Braak stages III and IV; subjects positive in Braak ROI I/II but negative elsewhere were assigned Braak stages I and II; and subjects negative across all 3 composite ROIs were assigned Braak stage 0.

Calculation of Normalized Hippocampal Volume

Hippocampal volume was reported as the percentage of the cerebral cortex to normalize across different participants, as calculated using the following equation (*20*):

$$\frac{\text{Volume of hippocampus}}{\text{Volume of cerebral cortex}} \times 100\% \qquad \text{Eq. 2}$$

Statistical Analyses

All statistical analyses were performed using SPSS Statistics, version 26.0 (IBM), and Matlab, version R2019b (MathWorks), to compare efAP values with tau PET positivity. All parametric analyses between Braak ROIs used the Pearson r correlation coefficient, whereas nonparametric analyses across all Braak stages used the Spearman ρ and nonparametric analyses between individual Braak stages used the Wilcoxon rank sum test. The significance level was a P value of less than 0.05 with a Bonferroni adjustment for multiple comparisons.

Intersubject, univariate Pearson correlations were performed between efAP and tau PET Braak ROIs I–VI across all 120 subjects, separating subjects by amyloid status. Because only 1 subject was positive in tau PET Braak ROI VI (SUVR > 1.22), this ROI was

TABLE 1
Cohort Demographics

Demographic	Amyloid-positive	Amyloid-negative
Total number of subjects	63	57
Tauopathy*		
Positive	36	7
Negative	27	50
Age (y)	74.36 ± 7.95	69.67 ± 7.71
Sex		
Male	25	24
Female	33	31
Formal education (y)	15.97 ± 2.55	15.85 ± 2.19
Apolipoprotein E-ε4		
Non-carrier of ε4 alleles	24	44
ε4/ε*	27	10
ε4/ε4	7	1
Mini-Mental State Examination† (*37*)	28.10 ± 2.83 (range, 18–30)	29.38 ± 1.01 (range, 25–30)
Clinical Dementia Rating (*36*)		
0 (not demented)	40	53
0.5 (uncertain or very mild dementia)	14	2
1 (mild dementia)	4	0
Amyloid–tau scan interval (d)	63.17 ± 67.86	63.93 ± 60.84

Apolipoprotein E-ε4 (ApoE4) carriers represented as number of ε4 alleles where ε4/ε stands for heterozygotes.
†Scores range from 30 (best) to 0 (worst).
Qualitative data are number; continuous data are mean ± SD. Of subjects used in study, 5 amyloid-positive and 2 amyloid-negative were missing demographic data and not included in table.

excluded for optimization purposes. Additionally for optimization purposes, and to align with our hypothesis, only the 63 amyloid-positive subjects were used. Area under the curve (AUC) was used to test the performance of the receiver-operating-characteristic (ROC) curve, with efAP being used as the predictor variable and tau positivity (SUVR > 1.22) in tau PET Braak ROIs I–V being used as the outcome variable. The early-frame interval and target ROI corresponding to the maximum AUC (mean ± SD) was selected for the remainder of the study. Similarly, the following 6 reference ROIs for the calculation of efAP were compared for the ability to predict positive tau PET findings: the entire cerebellum, the cerebral white matter, the region pre- and postcentral gyri, the Braak VI tau ROI, the Braak V/VI composite ROI, and the basal ganglia.

Logistic regression models were used to examine the accuracy of efAP in distinguishing between tau-negative and tau-positive groups. The performance of efAP was assessed using ROC curves to compare sensitivity and specificity and to determine the optimal cutoff for efAP and the best time interval. For parameter optimization for the dataset, AUC was calculated and compared with a value of 0.5 (random agreement) using the methods of Obuchowski et al. (*21*). Sensitivity, specificity, positive predictive value (PPV), and negative predictive value (NPV) were reported at the optimal cutoff based on the maximum Youden index (*22*). To evaluate performance between biomarkers in stratifying for tau positivity, ROC curves were compared using the methods of DeLong et al. (*23*), with SE as calculated by SPSS. Additionally, standardized net benefit was used to measure the improvement in efAP as an additional predictor over hippocampal volume, with tau PET positivity set as the outcome variable (*24*,*25*).

RESULTS

The Hippocampus Is Selected as the Optimal Target ROI, and the Cerebral White Matter Is Selected as the Optimal Reference ROI

Our first objective was to determine which target ROI, reference ROI, and time frames would optimize the predictive performance of efAP. When evaluating efAP as the predictor variable for each of the 79 ROIs and tau positivity as the outcome variable, we found that efAP in tau PET Braak ROI II (hippocampus) showed the strongest AUC across Braak ROIs I–V when using a cerebral white matter reference ROI (0.79 ± 0.082), peaking at 0.89 for tau PET using Braak ROI III (Fig. 2; Supplemental Figs. 1 and 2; supplemental materials are available at http://jnm.snmjournals.org). Thus, the hippocampus was chosen as the target ROI and the cerebral white matter was chosen as the reference ROI for efAP calculations for the remainder of the study.

The Optimal Early-Phase Interval Starts at 5% of Cerebral Cortex Peak Activity and Ends at 3 Minutes After Injection

Next, we determined which dynamic amyloid PET early time interval was most closely associated with tau PET. Using ROC analysis, we compared the AUCs when applying hippocampal efAP as the predictor variable and tau PET positivity across tau PET Braak ROIs I–V as the outcome variables (Supplemental Fig. 3). The endpoint of the early-phase interval was determined to be ideal at 3 min after injection, when the AUC was highest (0.79 ± 0.0042). Selection of the endpoint showed only a 3.3%

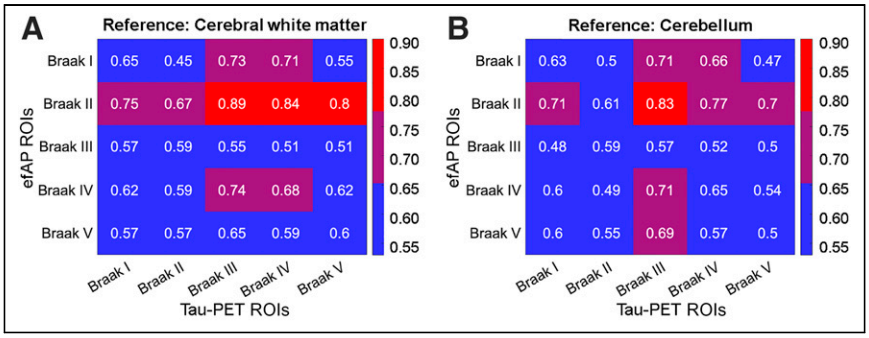

FIGURE 2. efAP Braak II ROI (hippocampus) and cerebral white matter chosen as target and reference ROIs, respectively. AUC was used to test performance of ROC curve. AUC between first 5 tau PET Braak ROIs shown for efAP was used as predictor variable, and tau PET was used as outcome variable. Different reference ROIs for calculation of efAP were compared with cerebral white matter (A) and cerebellum (B), showing strongest AUC across efAP in Braak II ROIs, also known as hippocampus. Color scale shows ranges of AUCs in tables, with blue being lowest, purple intermediate, and red highest.

decline from this peak AUC until 6 min after injection and a 8.5% decline until 10 min after injection, emphasizing the relative stability of efAP measurement to varying time intervals. Although altering the start point of the early-phase interval showed only marginal variations in the AUC (<5%), setting a higher threshold of peak cerebral cortex activity for selection of the first frame used in efAP measurement marginally decreased the AUC at all points (Supplemental Fig. 3). Thus, the early-phase interval starting at 5% of cerebral cortex peak activity and ending at 3 min after injection was deemed optimal.

Hippocampal efAP Correlates with Tau PET Results in Amyloid-Positive Participants

Next, we evaluated the relationships between hippocampal efAP and tau PET. A visual example of the inverse correlation between hippocampal efAP and tau PET for a cognitively normal subject (tau PET Braak stage 0) and for late-stage disease (tau PET Braak stages V and VI) is shown in Figure 3. Comparing hippocampal efAP with the tauopathy summary measure showed a significant Pearson correlation coefficient in amyloid-positive participants ($r = –0.57$, $P < 0.0001$). As expected, this relationship was absent in amyloid-negative participants (Fig. 4). Significant regional correlations ($P < 0.001$) were also seen in amyloid-positive participants across tau PET Braak ROIs I, II, III, IV, and V ($r = –0.50$, –0.43, –0.58, –0.66, and –0.48, respectively; Supplemental Fig. 4). ROC analysis revealed that hippocampal efAP could be used to strongly predict tau positivity on tau PET in amyloid-positive participants at a global level using the tauopathy summary measure (AUC, 0.86; efAP cutoff, 1.06; sensitivity, 71%; specificity, 93%; PPV, 93%; and NPV, 72%; Fig. 5A). Regional analyses in individual Braak ROIs I, II, III, IV, and V also showed strong discrimination of tau PET positivity (AUCs of 0.75, 0.67, 0.89, 0.84, and 0.80, respectively; Supplemental Fig. 5).

Hippocampal efAP Shows Stronger Correlation with Tau Status Than Does Hippocampal Volume

A reduction in hippocampal volume could reduce SUVs because of partial-volume averaging. Therefore, we compared these 2 biomarkers in amyloid-positive individuals to determine whether hippocampal efAP conveyed additional information not provided by hippocampal volume measurement alone. Characterizing subjects by their tau PET Braak stage showed that both hippocampal efAP and hippocampal volume significantly decreased with increasing tau PET Braak stage (Fig. 6). Hippocampal efAP showed a stronger inverse relationship with tau PET Braak stage ($\rho = –0.58$, $P < 0.0001$; Fig. 6A) than with hippocampal volume ($\rho = –0.37$, $P = 0.0034$; Fig. 6B). Wilcoxon rank sum testing between individual groups showed similar results, with the differences between Braak stages I and II and Braak stages III and IV being the greatest for both hippocampal efAP (1.11 ± 0.07 vs. 1.00 ± 0.07,

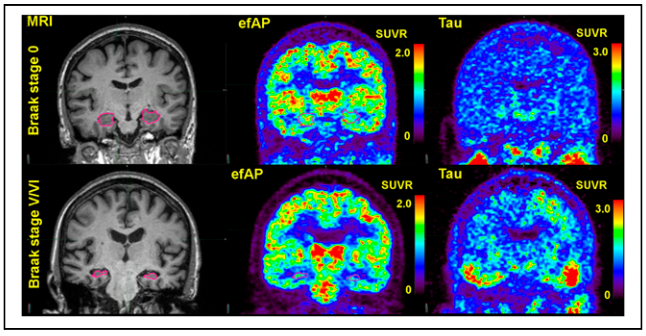

FIGURE 3. Example of inverse relationship between hippocampal efAP and tau PET Braak stage. Comparisons of representative subjects from tau PET Braak stage 0 and Braak stages V and VI show appearance of efAP at 2 ends of disease spectrum. First column highlights hippocampus in pink on volumetric MRI, second column shows efAP values from dynamic florbetapir PET, and third column shows tau PET. Intensity scales for PET images are shown as SUVRs.

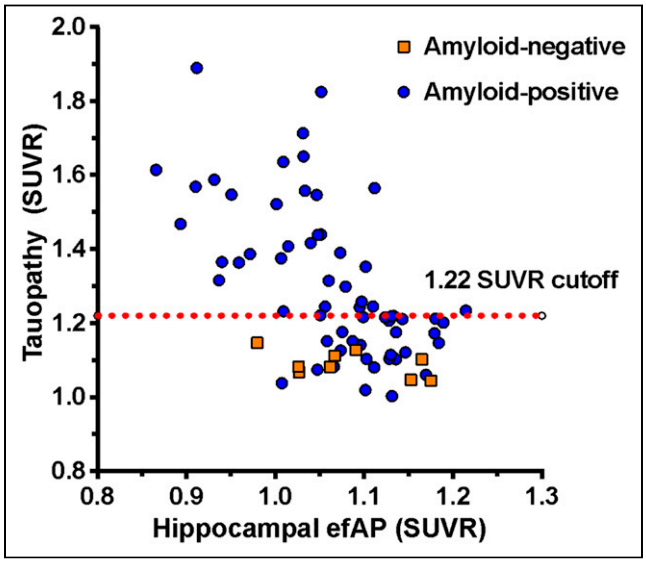

FIGURE 4. Comparison of hippocampal efAP and tau PET tauopathy summary measure for amyloid-positive ($r = –0.57$, $P < 0.0001$) and amyloid-negative ($r = 0.05$, $P = 0.69$) participants. efAP parallels and predicts tau PET pathology. Tau PET SUVR cutoff was used to stratify subjects for tau positivity.

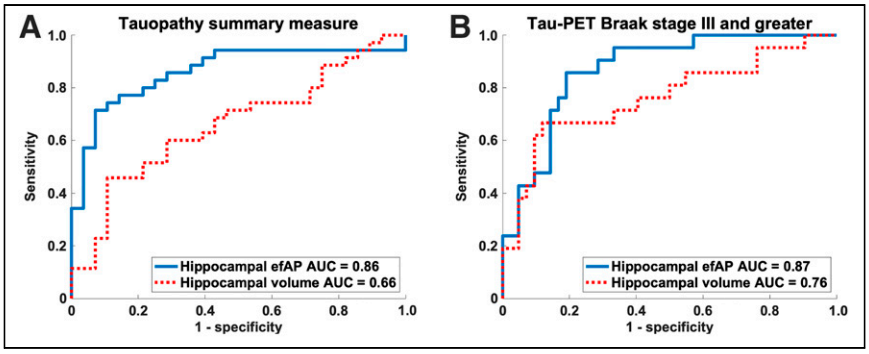

FIGURE 5. Predictor variables: ROC curves for efAP and normalized hippocampal volume. Outcome variables: tau PET positivity in tauopathy summary measure and Braak stage III or greater. Hippocampal efAP has stronger discriminatory ability than hippocampal volume for predicting tau PET positivity in amyloid-positive subjects. Tau positivity was defined as SUVR > 1.22. (A) AUC measured for efAP cutoff of 1.06 was 0.86, with sensitivity and specificity of 71% and 93%, respectively, and PPV and NPV of 93% and 72%, respectively; AUC measured for volume was 0.66, with sensitivity and specificity of 46% and 89%, respectively, and PPV and NPV of 84% and 57%, respectively. AUC difference was statistically significant ($z = 3.08$, $P = 0.002$). (B) AUC measured for efAP cutoff of 1.05 was 0.87, with sensitivity and specificity of 86% and 81%, respectively, and PPV and NPV of 69% and 92%, respectively; AUC measured for volume was 0.76, with sensitivity and specificity of 67% and 88%, respectively, and PPV and NPV of 74% and 84%, respectively. This AUC difference did not reach statistical significance ($z = 1.54$, $P = 0.12$).

$P = 0.0002$; Fig. 6A) and hippocampal volume (1.86 ± 0.18 vs. 1.60 ± 0.20, $P = 0.0014$; Fig. 6B). When looking at efAP and hippocampal volume as individual predictors of tau PET, the discriminatory ability to predict tau positivity was superior for hippocampal efAP compared with hippocampal volume across the tauopathy summary measure (AUC, 0.86 vs. 0.66; $z = -3.08$; $P = 0.002$) with higher sensitivity (71% vs. 46%), specificity (93% vs. 89%), PPV (93% vs. 84%), and NPV (72% vs. 57%) (Fig. 5A). Although hippocampal efAP showed a trend toward higher predictive ability than hippocampal volume for Braak stage III or greater, the results did not reach statistical significance (AUC, 0.87 vs. 0.76; $z = 1.54$; $P = 0.12$; Fig. 5B).

Similarly, when efAP and volume were grouped as copredictors of tau positivity, efAP showed a significant, additive benefit to simply using hippocampal volume alone to predict tau positivity when utilizing tauopathy summary ROI (Δ standardized net benefit, 0.3472; $P = 0.0070$) but not when utilizing Braak stage III or greater positivity (Δ standardized net benefit, 0.0998; $P = 0.38$).

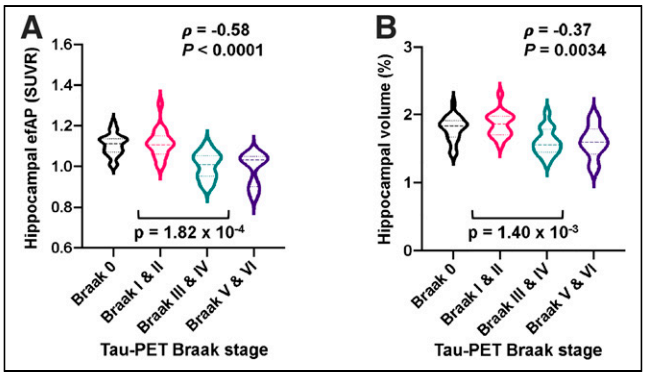

FIGURE 6. Amyloid-positive participants stratified by tau PET Braak stage and violin plots displayed for hippocampal efAP (A) and normalized hippocampal volume (B). Tau PET Braak stage shows stronger association with efAP than with volume within hippocampus. Spearman rank ρ was used to test for association across all groups, and Wilcoxon rank sum test was used to test for association between individual groups, with $P < 0.05$ denoted as significant.

DISCUSSION

Hippocampal efAP, a biomarker related to flow during the early frames of dynamic amyloid PET, correlates with tau PET in amyloid-positive individuals. Hippocampal efAP shows promise for predicting tau pathology measured with ^{18}F-flortaucipir PET and—in predicting tau pathology—provides significant, additive utility over hippocampal volume alone. The use of efAP could add specificity to the assessment of AD with amyloid PET and allow a more comprehensive neuroimaging examination.

Our cross-sectional retrospective analysis demonstrated a strong, significant association between hippocampal efAP and tau PET Braak stage (Fig. 6A). Our results also showed that hippocampal efAP had strong discriminatory performance in assessing tau positivity at the optimal cutoff, based on the maximum Youden index (*22*), whether using either a validated tauopathy measure (*15*) or Braak staging. For instance, hippocampal efAP had a high PPV (93%) and moderate NPV (72%) in amyloid-positive individuals, compared with the tauopathy summary measure with ^{18}F-flortaucipir PET. The SUVR threshold for tau positivity (1.22) used in this study was based on the previously conducted study at the Charles F. and Joanne Knight Alzheimer Disease Research Center (*15*). This SUVR threshold may vary with the population and PET study parameters but likely will fall within a fairly narrow range based on studies by other groups, which reported optimal cutoffs ranging from 1.23 to 1.27 (*26–28*).

Among the 79 target ROIs evaluated for efAP, the hippocampus provided the strongest predictive power for tau positivity. Identification of the hippocampus as the most accurate target ROI for efAP was somewhat surprising, as the precuneus and posterior cingulate gyrus show hypometabolism (*29*) and hypoperfusion (*30*) early in the course of AD. Previous research has explored mainly direct, one-to-one regional correlations between ^{18}F-FDG PET and tau PET (*12*,*13*,*31*) and between ^{18}F-FDG PET and perfusion (*9–11*,*32*), and it is recognized that spatial differences exist between ^{18}F-FDG and tau PET (*31*), such as in the hippocampus, where hypometabolism does not correlate well with tau pathology (*12*). Alternative methods for estimating perfusion from dynamic amyloid PET exist, such as pharmacokinetic modeling (*11*,*33*). In particular, Joseph-Mathurin et al. noted that pharmacokinetics-derived R1 values from ^{11}C-Pittsburgh compound B spatially correlated with ^{18}F-FDG PET but that early-frame intervals did not (*33*).

We found that the optimal early-frame time window started at 5% of peak cerebral cortex activity and ended at 180 s after injection. Importantly, efAP was found to be relatively stable up to 6 and 10 min, with small reductions in AUC. Our results were similar to another ^{18}F-florbetapir study that evaluated the performance of early-frame dynamic amyloid PET imaging compared with ^{18}F-FDG PET, in which the 1- to 6-min time window provided the

best surrogate for perfusion based on ^{18}F-FDG PET (*32*). Several other studies that used ^{11}C-Pittsburgh compound B instead of ^{18}F-florbetapir showed similar results (*6*,*10*,*11*,*34*). One of these studies, in particular, corroborated our results by finding that a shorter interval, specifically 20–130 s after injection, best discriminated between AD patients and controls even though with ^{18}F-FDG PET a longer interval correlated better (*10*). Our efAP method focused on quantitative analysis rather than visual interpretation, and it is possible that a longer interval would be more suitable for visual analysis by reducing image noise.

Reduction in hippocampal volume, as measured by MRI, has been robustly validated and remains one of the core biomarkers in AD because of strong evidence supporting its diagnostic and prognostic value (*2*,*35*). In our present study, decreases in both hippocampal efAP and hippocampal volume were shown to be inversely correlated with tau PET Braak staging. On the basis of the tauopathy summary measure, hippocampal efAP was a better predictor of tau positivity than was hippocampal volume measurement alone, with additive benefit. A trend toward better performance with hippocampal efAP than with hippocampal volume ($P = 0.12$) was observed for Braak stage III or higher but did not reach statistical significance. The relatively small number of participants with elevated tau in Braak ROI III or higher ($n = 21$) prevents a definitive conclusion regarding the additional value of hippocampal efAP versus hippocampal volume for individual Braak stages.

Our work has limitations that are important to address in future work. Our study population included a large proportion of amyloid-positive subjects who were cognitively normal or had mild cognitive impairment. Our efAP results, including the optimal brain ROI for efAP measurement, may be different in individuals with more advanced AD. For the hippocampal efAP analysis, we chose to focus on amyloid-positive subjects because ^{18}F-flortaucipir is best suited for imaging the pathologic form of tau that is deposited in AD. Our evaluation of the amyloid-negative subjects was more limited because this group is potentially heterogeneous and is not expected to have many individuals positive for tau based on ^{18}F-flortaucipir PET. The PET tracer injection technique was not optimized for the early-frame measurement of efAP. Although exclusion criteria did help by removing subjects if the bolus perfusion phase was inadequate based on their time to peak (>150 s), the time to peak for included subjects still varied widely, from 45 to 150 s. Our findings suggest that efAP was not highly sensitive to differences in the rate of bolus delivery, but future studies would benefit from a more standardized injection technique.

CONCLUSION

We have shown that efAP acquired concurrently with a standard amyloid PET study is a strong predictor of tau pathology in amyloid-positive individuals. Successful development of this approach has the potential to provide information on both amyloid and tau pathology in a single PET session, which may reduce imaging costs and the burden on patients and their families.

DISCLOSURE

This work was supported by National Institutes of Health grants P20AG068024, RF1AG059009, and T32GM008361; the Medical Science Training Program, the Alzheimer Drug Discovery Foundation, and the Department of Radiology at the University of Alabama at Birmingham. Tammie Benzinger is funded by NIH grants P50AG005681, P01AG003991, P01AG026276, UF01AG032438, R01AG05326, RF1AG053550, R01AG054567, and R01AG052550. John Morris is funded by NIH grants P50AG005681, P01AG003991, P01AG026276, and UF01AG032438. The recruitment of participants and their clinical characterization and neuroimaging were supported by NIH grants P50AG05681, P01AG03991, and P01AG026276. Avid Radiopharmaceuticals, which is a wholly owned subsidiary of Eli Lilly (^{18}F-florbetapir and ^{18}F-flortaucipir imaging), provided the ^{18}F-florbetapir doses and partial support for ^{18}F-florbetapir scanning through an investigator-initiated research grant awarded to Washington University (John Morris and Tammie Benzinger); provided technology transfer; and provided precursor for ^{18}F-florbetapir. Jonathan McConathy has declared a relationship with Eli Lilly and Avid, to which he provides consulting and from which he receives research support. No other potential conflict of interest relevant to this article was reported.

ACKNOWLEDGMENTS

Data used in the preparation of this article were obtained from the Charles F. and Joanne Knight Alzheimer Disease Research Center at the Washington University in St. Louis and are available on request (https://knightadrc.wustl.edu/). ^{18}F-flortaucipir was produced under a material transfer agreement between Washington University and Avid Radiopharmaceuticals.

KEY POINTS

QUESTION: Do the first few frames after tracer injection on dynamic amyloid PET predict tau pathology on tau PET in amyloid-positive participants?

PERTINENT FINDINGS: This retrospective study showed that decreased activity in the hippocampus as measured with efAP predicts tau pathology on tau PET in amyloid-positive individuals.

IMPLICATIONS FOR PATIENT CARE: Our findings show that efAP may facilitate prediction of tau status from an amyloid PET study and provide a more comprehensive neuroimaging assessment of cognitive impairment, with increased specificity for AD.

REFERENCES

1. Jack CR Jr, Bennett DA, Blennow K, et al. NIA-AA research framework: toward a biological definition of Alzheimer's disease. *Alzheimers Dement.* 2018;14:535–562.
2. Jack CR Jr, Wiste HJ, Weigand SD, et al. Age-specific and sex-specific prevalence of cerebral beta-amyloidosis, tauopathy, and neurodegeneration in cognitively unimpaired individuals aged 50-95 years: a cross-sectional study. *Lancet Neurol.* 2017;16:435–444.
3. Richards D, Sabbagh MN. Florbetaben for PET imaging of beta-amyloid plaques in the brain. *Neurol Ther.* 2014;3:79–88.
4. Wong DF, Rosenberg PB, Zhou Y, et al. In vivo imaging of amyloid deposition in Alzheimer disease using the radioligand ^{18}F-AV-45 (florbetapir F 18). *J Nucl Med.* 2010;51:913–920.
5. Ossenkoppele R, Prins ND, van Berckel BN. Amyloid imaging in clinical trials. *Alzheimers Res Ther.* 2013;5:36.
6. Blomquist G, Engler H, Nordberg A, et al. Unidirectional influx and net accumulation of PIB. *Open Neuroimag J.* 2008;2:114–125.
7. Forsberg A, Engler H, Blomquist G, Langstrom B, Nordberg A. The use of PIB-PET as a dual pathological and functional biomarker in AD. *Biochim Biophys Acta.* 2012;1822:380–385.
8. Chen YJ, Rosario BL, Mowrey W, et al. Relative ^{11}C-PiB delivery as a proxy of relative CBF: quantitative evaluation using single-session ^{15}O-water and ^{11}C-PiB PET. *J Nucl Med.* 2015;56:1199–1205.

9. Rodriguez-Vieitez E, Leuzy A, Chiotis K, Saint-Aubert L, Wall A, Nordberg A. Comparability of [^{18}F]THK5317 and [^{11}C]PIB blood flow proxy images with [^{18}F]FDG positron emission tomography in Alzheimer's disease. *J Cereb Blood Flow Metab.* 2017;37:740–749.
10. Peretti DE, Vallez Garcia D, Reesink FE, et al. Relative cerebral flow from dynamic PIB scans as an alternative for FDG scans in Alzheimer's disease PET studies. *PLoS One.* 2019;14:e0211000.
11. Rodriguez-Vieitez E, Carter SF, Chiotis K, et al. Comparison of early-phase ^{11}C-deuterium-L-deprenyl and ^{11}C-Pittsburgh compound B PET for assessing brain perfusion in Alzheimer disease. *J Nucl Med.* 2016;57:1071–1077.
12. Bischof GN, Jessen F, Fliessbach K, et al. Impact of tau and amyloid burden on glucose metabolism in Alzheimer's disease. *Ann Clin Transl Neurol.* 2016;3:934–939.
13. Whitwell JL, Graff-Radford J, Tosakulwong N, et al. Imaging correlations of tau, amyloid, metabolism, and atrophy in typical and atypical Alzheimer's disease. *Alzheimers Dement.* 2018;14:1005–1014.
14. Berg L, McKeel DW Jr, Miller JP, et al. Clinicopathologic studies in cognitively healthy aging and Alzheimer's disease: relation of histologic markers to dementia severity, age, sex, and apolipoprotein E genotype. *Arch Neurol.* 1998; 55:326–335.
15. Mishra S, Gordon BA, Su Y, et al. AV-1451 PET imaging of tau pathology in preclinical Alzheimer disease: defining a summary measure. *Neuroimage.* 2017;161: 171–178.
16. Su Y, Flores S, Wang G, et al. Comparison of Pittsburgh compound B and florbetapir in cross-sectional and longitudinal studies. *Alzheimers Dement (Amst).* 2019;11: 180–190.
17. Fischl B, Salat DH, Busa E, et al. Whole brain segmentation: automated labeling of neuroanatomical structures in the human brain. *Neuron.* 2002;33:341–355.
18. Raman F, Grandhi S, Murchison CF, et al. Biomarker localization, analysis, visualization, extraction, and registration (BLAzER) methodology for research and clinical brain PET applications. *J Alzheimers Dis.* 2019;70:1241–1257.
19. Schöll M, Lockhart SN, Schonhaut DR, et al. PET imaging of tau deposition in the aging human brain. *Neuron.* 2016;89:971–982.
20. Risacher SL, Anderson WH, Charil A, et al. Alzheimer disease brain atrophy subtypes are associated with cognition and rate of decline. *Neurology.* 2017;89:2176–2186.
21. Obuchowski NA, Lieber ML, Wians FH Jr. ROC curves in clinical chemistry: uses, misuses, and possible solutions. *Clin Chem.* 2004;50:1118–1125.
22. Habibzadeh F, Habibzadeh P, Yadollahie M. On determining the most appropriate test cut-off value: the case of tests with continuous results. *Biochem Med (Zagreb).* 2016;26:297–307.
23. DeLong ER, DeLong DM, Clarke-Pearson DL. Comparing the areas under two or more correlated receiver operating characteristic curves: a nonparametric approach. *Biometrics.* 1988;44:837–845.
24. Vickers AJ, Elkin EB. Decision curve analysis: a novel method for evaluating prediction models. *Med Decis Making.* 2006;26:565–574.
25. Pepe MS, Fan J, Feng Z, Gerds T, Hilden J. The net reclassification index (NRI): a misleading measure of prediction improvement even with independent test data sets. *Stat Biosci.* 2015;7:282–295.
26. McSweeney M, Pichet Binette A, Meyer PF, et al. Intermediate flortaucipir uptake is associated with Aβ-PET and CSF tau in asymptomatic adults. *Neurology.* 2020; 94:e1190–e1200.
27. Ossenkoppele R, Rabinovici GD, Smith R, et al. Discriminative accuracy of [^{18}F]flortaucipir positron emission tomography for Alzheimer disease vs other neurodegenerative disorders. *JAMA.* 2018;320:1151–1162.
28. Dodich A, Mendes A, Assal F, et al. The A/T/N model applied through imaging biomarkers in a memory clinic. *Eur J Nucl Med Mol Imaging.* 2020;47:247–255.
29. Kato T, Inui Y, Nakamura A, Ito K. Brain fluorodeoxyglucose (FDG) PET in dementia. *Ageing Res Rev.* 2016;30:73–84.
30. Ishii K, Sasaki M, Yamaji S, Sakamoto S, Kitagaki H, Mori E. Demonstration of decreased posterior cingulate perfusion in mild Alzheimer's disease by means of $H_2{}^{15}O$ positron emission tomography. *Eur J Nucl Med.* 1997;24:670–673.
31. Ossenkoppele R, Schonhaut DR, Scholl M, et al. Tau PET patterns mirror clinical and neuroanatomical variability in Alzheimer's disease. *Brain.* 2016;139:1551–1567.
32. Hsiao IT, Huang CC, Hsieh CJ, et al. Correlation of early-phase ^{18}F-florbetapir (AV-45/Amyvid) PET images to FDG images: preliminary studies. *Eur J Nucl Med Mol Imaging.* 2012;39:613–620.
33. Joseph-Mathurin N, Su Y, Blazey TM, et al. Utility of perfusion PET measures to assess neuronal injury in Alzheimer's disease. *Alzheimers Dement (Amst).* 2018; 10:669–677.
34. Gietl AF, Warnock G, Riese F, et al. Regional cerebral blood flow estimated by early PiB uptake is reduced in mild cognitive impairment and associated with age in an amyloid-dependent manner. *Neurobiol Aging.* 2015;36:1619–1628.
35. Pini L, Pievani M, Bocchetta M, et al. Brain atrophy in Alzheimer's disease and aging. *Ageing Res Rev.* 2016;30:25–48.
36. Morris JC. The Clinical Dementia Rating (CDR): current version and scoring rules. *Neurology.* 1993;43:2412–2414.
37. Folstein MF, Folstein SE, McHugh PR. "Mini-mental state": a practical method for grading the cognitive state of patients for the clinician. *J Psychiatr Res.* 1975; 12:189–198.